High-resolution x-ray scattering study of the effect of quenched random disorder on the nematic–smectic-*A* transition

M. Ramazanoglu,[1,4] S. Larochelle,[1] C. W. Garland,[2] and R. J. Birgeneau[1,3]
[1]*Department of Physics, University of Toronto, Ontario M5S 1A7, Canada*
[2]*Department of Chemistry, Massachusetts Institute of Technology, Cambridge, Massachusetts 02139, USA*
[3]*Department of Physics, University of California, Berkeley and Lawrence Berkeley National Laboratory, California 94720, USA*
[4]*Department of Physics and Astronomy, McMaster University, Hamilton, L8S 4M1, Canada*
(Received 12 September 2006; revised manuscript received 28 March 2007; published 14 June 2007)

Using high-resolution x-ray scattering, the effect of quenched random disorder (QRD) on the second-order nematic–smectic-*A* (*N*-Sm*A*) phase transition in butyloxybenzilidene-octylaniline (4O.8) has been studied. 4O.8 is a nonpolar liquid crystal (LC) with a monomeric smectic-*A* phase. The QRD is created by aerosil nanoparticles which gelate to form a three-dimensional network, confining the LC. The QRD caused by the aerosil gel generates quenched random fields acting on both the nematic and smectic-*A* order parameters. This results in the destruction of the quasi-long-range order of the smectic-*A* phase. The x-ray scattering data are modeled with a structure factor composed of two terms, one thermal and one static, corresponding to the connected and disconnected susceptibilities, respectively. Unlike previous studies, the two parts of the structure factor are decoupled by allowing different thermal and static correlation lengths. Our fitting procedure involves temperature-dependent and temperature-independent (global) variables. The amplitude and the parallel correlation length for the thermal part of the line-shape show critical-like behavior both above and below the transition temperature. Detailed analysis reveals that the thermal correlation length does not truly diverge at the phase transition. This effect is discussed on the basis of a cutoff for the divergence caused by the random fields generated by the aerosil network confining the liquid crystal. The intensity of the static term in the line-shape behaves like the order parameter squared at a conventional second-order phase transition. The effective order parameter critical exponent shows an evolution with increasing aerosil gel density ranging from the Gaussian tricritical value to the 3D-*XY* value. The results of a pseudocritical scaling analysis are compared to an analysis of 4O.8+aerosil heat capacity data and discussed using a phenomenological correlation between the nematic range of pure liquid crystals and the aerosil mass density, ρ_s.

DOI: 10.1103/PhysRevE.75.061705 PACS number(s): 64.70.Md, 61.30.Eb, 61.10.−i

I. INTRODUCTION

The effects of random disorder on phase transitions have been studied in liquid crystals for more than a decade [1]. Liquid crystals (LCs) are interesting because of their rich variety of phases. Of course, all LCs have impurities but these typically impose *annealed* disorder on LC phase transitions. However, it has been observed that with appropriate care, mixtures of some thermotropic LCs and aerosil nanoparticles can form a gel phase with the aerosil partial volume fraction as low as 0.01. The resultant aerosil network acts as a source of *quenched* random disorder (QRD) on any LC phase transitions. The aerosil density may be varied by more than a factor of 10. The density of the aerosil can be directly associated with the strength of the quenched disorder imposed on the LC [2]. The earliest works in this field focused on the closely related system of LC+aerogel mixtures [1,3,4], where the LC is injected into an aerogel. Aerogels were previously known to have interesting effects on phase transitions from the numerous studies which had been conducted on both the ^{4}He+aerogel system and ^{4}He-^{3}He binary liquid mixtures embedded in aerogels [5].

In LC+aerogel systems, where the gel couples directly to the smectic LC order parameter, the resultant disorder is quite large because of the rigid chemically bonded structure of aerogels and the nematic–smectic-*A* transition features are severely smeared. Therefore, the interesting pseudocritical thermal properties are largely masked by the static random fluctuations [6,7]. Furthermore, aerogels only allow the exploration of a limited range of gel densities. For these reasons, we have used aerosils, which are ~7-nm-diameter spherical nanoparticles covered with hydroxyl groups on their surfaces, instead of aerogels to study the effects of QRD on the nematic–smectic-*A* (*N*-Sm*A*) phase transition. It is found that aerosils perturb the host material in a less destructive way than aerogels [7,8]. Because one can produce stable gels with an aerosil volume fraction as low as 0.01, it is possible to control the QRD effects to quite low levels. This makes the study of LC+aerosil gels particularly interesting. It should also be noted that the weak hydrogen-bond interactions between aerosil particles may allow some reshaping of the aerosil network as the LC changes phases; that is, there may be some partial annealing of the disorder [9]. There is some indirect but not conclusive evidence for such partial annealing. The effect of correlated disorder was discussed by Weinberg and Halperin [10]. However, this will not alter the fundamental nature of the phases and the phase transitions [11]. LC+aerosil mixtures have been studied using a number of different techniques including nuclear magnetic resonance (NMR)[12], dielectric susceptibility [13], light scattering [14], and calorimetry [7,8,15].

The effects of the aerosil gel confinement on the *N*-Sm*A* phase transition have been studied in detail using x-ray scattering techniques in 8CB+aerosil and 8OCB+aerosil gels

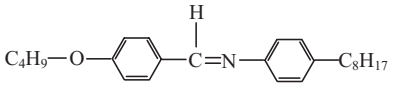

FIG. 1. Structure of 4O.8 LC. 4O.8 is a nonpolar LC with a monomeric smectic-A_m phase.

[16–20]. Unlike 4O.8, both 8CB and 8OCB have incommensurate partial bilayer SmA_d phases, caused by the cyano group on one end of the molecule. From these pioneering experiments, it has been observed that even the weak quenched disorder introduced by a low-density aerosil gel destroys the quasi-long-range order (i.e., quasi is due to the Landau-Peierls instability [21]) in the Sm*A* phase and instead produces a short-range-ordered (SRO) state. This result is seen even for a gel mixture containing the lowest amount of silica aerosil, with mass density $\rho_s = 0.022$ g/cm^3 [22] which corresponds to a volume fraction of 0.01. This density is just above the gelation threshold of $\rho_s \cong 0.015$ g/cm^3. These results are consistent with the theoretical studies of Radzihovsky and Toner [11] as we shall discuss in Sec. IV of this paper.

The molecular formula for 4O.8, a monomeric smectic-A_m phase liquid crystal, is shown schematically in Fig. 1. The phase transition sequence for pure 4O.8 is given as [8]

$$\underset{\sim 311.2\ \mathrm{K}}{\mathrm{Cr}K} \leftarrow \underset{\sim 322.6\ \mathrm{K}}{\mathrm{Cr}B} \leftarrow \underset{\sim 336.9\ \mathrm{K}}{\mathrm{Sm}A} \leftarrow \underset{\sim 352\ \mathrm{K}}{N} \leftarrow I\,,$$

where *I*, *N*, Sm*A*, Cr*B*, and Cr*K* stand for the isotropic, nematic, smectic-*A*, crystalline *B*, and crystalline *K* phases, respectively.

In previous studies, an x-ray scattering structure factor composed of the spherical average of a Lorentzian and its squared form was chosen to characterize the SRO in the Sm*A* phase. These two terms are the thermal and static fluctuation structure factors corresponding to the connected and disconnected susceptibilities, respectively. Above the *N*-Sm*A* effective transition temperature $T^*(\rho_s)$, only the Lorentzian part of the structure factor was necessary to model the scattering data. In this temperature range, thermal critical smectic-*A* fluctuations in the nematic phase were observed. Below the transition temperature, both terms in the line shape were required to model the data. The amplitudes of the structure factors and the parallel correlation length were fitted as functions of temperature. In these fits, a strong correlation was observed between the amplitudes and the correlation length which made the analysis difficult [16–18]. In order to stabilize the analysis in the 8CB+aerosil study, the thermal amplitude was held at a constant value for $T^* < T$. This way, it was possible to obtain consistent behavior between the intensity of the random term and the aerosil mass density [19]. The same problem manifested itself as large nonmonotonic variations of the thermal amplitude and the correlation length in the *N*-Sm*A* transition in the 8OCB +aerosil study [18].

In the current study, a different approach has been followed to analyze the data. First and most importantly, the Lorentzian and Lorentzian squared terms of the structure factor are allowed to have independent correlation lengths. Second, some of the parameters are assumed to be temperature independent. These are fitted to a global value which is the same for all of the data. Third, all of the scans for a given ρ_s are analyzed simultaneously, thus giving optimal values for the global parameters.

In this study, the short-range Sm*A* order in 4O.8+aerosil gels is studied using high-resolution x-ray scattering as noted above. The results are discussed on the basis of the three-dimensional (3D) *XY* model in the presence of a random field [16,17,36]. A linear scaling between the aerosil mass density and the McMillan ratio for pure LCs is used to compare the extracted exponents from the analyses of x-ray scattering and heat capacity experiments.

In Sec. II, we present various experimental details including sample preparation and the x-ray scattering measurements. In Sec. III, the experimental results and the details of the line-shape analysis are presented. Section IV presents a scaling analysis of the x-ray data with comparisons to heat capacity experiment results.

II. EXPERIMENTS AND METHODS

A. Sample preparation

The 4O.8 LC was used as purchased from Frinton Lab [23] without any further purification. Hydrophilic type-300 aerosil, obtained from Degussa Corp [24], was used in this study. The nanoparticles of silica had a Brunauer-Emmet-Teller (BET) surface area of 300 m^2 g^{-1} and a diameter of roughly ~7 nm. Before being mixed with 4O.8, the aerosil particles were dried on a hot plate at ~300 °C under a rough vacuum (~10^{-2} atm) for at least 3 days. Stochiometric amounts of 4O.8 and dried aerosil particles were mixed in an absolute ethanol solution. The samples were characterized by the aerosil mass density ρ_s which is the ratio of aerosil mass in solution to the 4O.8 LC volume. Homogeneity of the mixture was achieved by sonicating the ethanol solution of 4O.8+aerosil for at least 1 h. The ethanol solvent was then removed by evaporation for one day at 75±1 °C, just below the boiling temperature of ethanol [25]. After drying, a small amount of mixture, about ~0.1 g, was placed into a LC cell using a hot spatula. The LC cells had Kapton windows of 5 mm diameter on the top and bottom of the cells in order to let the x-ray beam pass through the sample. After their transfer, the samples were left for several hours on the hot plate at 77±2 °C in order to anneal the mixture in case the aerosil network was mechanically perturbed during the cell filling. Most of the data were collected between the temperatures of 353 K and 323 K with the temperature decreasing. When necessary, subsequent runs were also taken in both cooling and heating directions especially near the phase transition. It was found that the data repeated themselves in both heating and cooling directions without any significant temperature hysteresis, consistent with the previous results [12]. This is in sharp contrast to the pronounced hysteresis seen in many experiments in random field Ising magnets (RFIMs) [26]. This reversibility also provides evidence that the samples were not significantly damaged by x rays during the exposure time used in the experiment, which was less than 2 h for each sample.

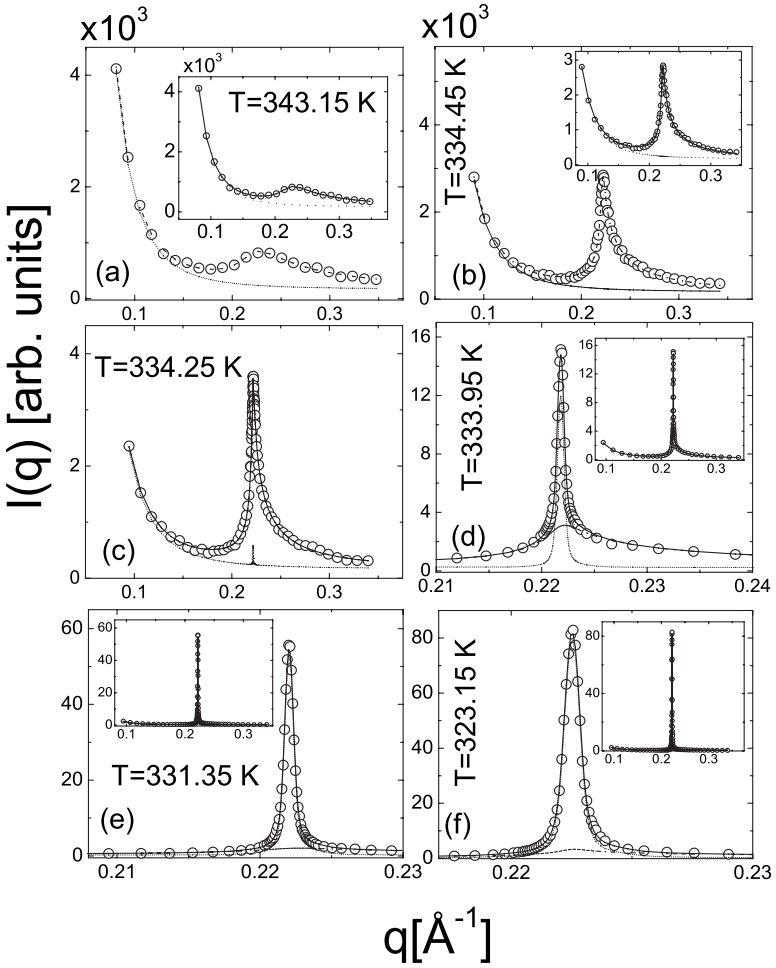

FIG. 2. Scattering intensity $I(q)$ for 4O.8 +aeosil gels with $\rho_s=0.040$ g/cm^3 (sample B). Panels are drawn to demonstrate the fit of the total structure factor, Eq. (2), represented by the solid lines. For panels (a) and (b), the data are modeled by the thermal part of the structure factor alone, which is shown by the dashed lines. For the four lowest temperatures, the static part contributes to the profile and grows rapidly on cooling (shown by the dotted lines). The thermal part is diminished in this temperature range (shown as dashed lines).

B. X-ray scattering

X-ray diffraction experiments were carried out at the National Synchrotron Light Source (NSLS) at Brookhaven National Laboratory (BNL). Beamlines X-20 A and X-22 A were used. These are bend magnet beamlines with Ge(111) and Si(111) monochromators, respectively. The synchrotron x-ray beam energy was tuned to 10 keV for X-20 A and 10.7 keV for X-22 A. The experiments were performed in transmission geometry with a vertical Θ-2Θ diffraction condition. The direct beam was measured after each temperature scan and used as the instrumental resolution function in the analysis. The momentum resolution was approximately $\Delta q \cong 0.001$ Å^{-1} [full width at half maximum (FWHM)] for both beamlines.

III. EXPERIMENTAL RESULTS AND ANALYSIS

Figure 2 shows the evolution of the smectic structure factor for a 4O.8+aerosil gel of $\rho_s=0.040$ g/cm^3 as the sample is cooled from near the isotropic phase through the nematic to smectic-A phase transition. The six different scans shown in this figure range in temperature from $T\cong 343$ K, where the sample is in the nematic phase, to $T\cong 323$ K, where the sample is deep in the smectic phase, just above the SmA-CrB transition. Most of the experiments were conducted within this temperature range. Higher-temperature data where the sample was in the I phase were also collected. These data were necessary to determine the global background function. For all of the 4O.8+aerosil samples, ranging from that with the lowest disorder $\rho_s=0.025$ g/cm^3 to that with the highest disorder $\rho_s=0.3$ g/cm^3, the smectic peaks are found to be broader than the instrumental resolution. This is illustrated in Fig. 3 for smectic peaks scanned at $T=323.15$ K, where the SmA_m phase is fully developed. As is evident in the figure, the smectic peak broadens progressively as the aerosil mass density ρ_s is increased. This confirms that the random field from the aerosil gel destroys the LRO of the smectic A_m phase; specifically, only SRO is observed in each of the samples even when the relative aerosil volume fraction is as low as 0.01. We will discuss the significance of these qualitative results below.

A. Line-shape analysis

Radzihovsky and Toner [11] have presented a comprehensive theory for the behavior of nematic and smectic-A LCs in a quenched random environment such as the LC+aerosil gel system. From the point of view of this paper, the most important feature of their theory is that the gel generates a random tilt field which couples linearly to the nematic director and a random positional field which couples linearly to the smectic-A order parameter. Radzihovsky and Toner further show that the fractal structure of the gel is irrelevant;

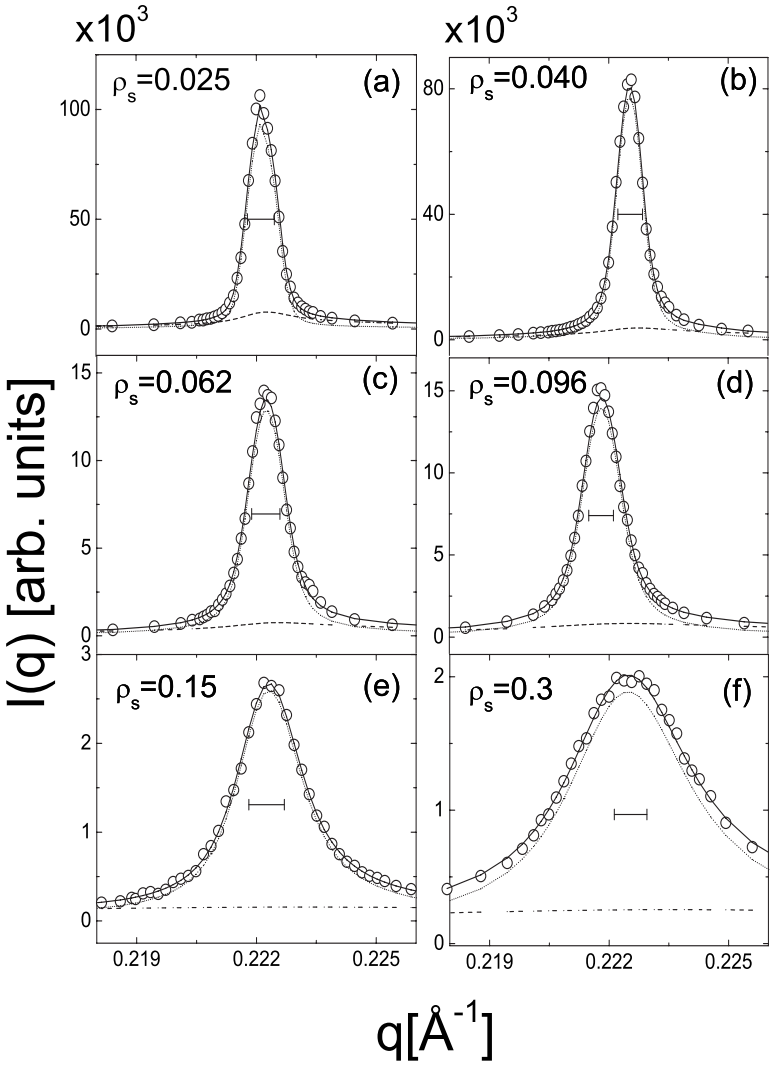

FIG. 3. Scattering intensity $I(q)$ for all 4O.8 +aerosil gels used in this study at the lowest experimental temperature, $T=323.15$ K. In the analysis, the whole data range [0.1–0.35] Å^{-1} is used; however, in order to show the resolution widths only the central part of the scans are shown. The solid lines show the total fit of the scattering structure factor, Eq. (2), plus the background. As seen in each panel, $S^{thermal}$ makes a significant contribution only to the tails while S^{static}, represented by dotted lines, defines the peak. The FWHM of the instrumental resolutions are shown with horizontal lines. In low- ρ_s samples [panels (a) and (b)] the resolutions widths are still slightly narrower than the smectic peaks.

that is, the smectic density wave will only be sensitive to the short-range disorder. Thus, as a good approximation, the *N*-Sm*A* phase transition in the LC+aerosil gel system should be a realization of the 3D *XY* model in a random field.

We now discuss a phenomenological model for the smectic-*A* structure factor. A structure factor composed of a Lorentzian plus a Lorentzian squared has been used previously to analyze random field systems—for example, random Ising magnets [26,27]. This structure factor is in part motivated by mean-field theory for quenched random field systems where the order parameter couples linearly to a random field. As noted above, the aerosil particles will fix the phase of the smectic mass density wave and hence act as a source of random fields. In a single crystal or more generally a system with orientational long-range order, the structure factor is given by

$$S(\boldsymbol{q}) = S^{thermal}(\boldsymbol{q}) + S^{static}(\boldsymbol{q}), \tag{1a}$$

where

$$S^{thermal}(\boldsymbol{q}) = \frac{\sigma_1}{1 + (q_\parallel - q_0)^2 \xi_\parallel^2 + q_\perp^2 \xi_\perp^2 + c q_\perp^4 \xi_\perp^4}, \tag{1b}$$

$$S^{static}(\boldsymbol{q}) = \frac{a_2(\xi_\parallel \xi_\perp^2)}{[1 + (q_\parallel - q_0)^2 \xi_\parallel^2 + q_\perp^2 \xi_\perp^2 + c q_\perp^4 \xi_\perp^4]^2}. \tag{1c}$$

Equation (1a) must be spherically averaged to describe the smectic fluctuations in the LC+aerosil gel system which has only short-range orientational order and hence is orientationally isotropic. Equation (1b) describes the thermal fluctuations while the second term given in Eq. (1c) describes the static fluctuations due to the random field. These parts of the structure factor correspond to the connected and disconnected susceptibilities, respectively.

In the equations above, $q_0 = 2\pi/d$ is the position of the peak corresponding to the smectic layer thickness d. $q_\parallel$ is the scattering momentum component parallel to the smectic mass density wave vector—that is, the component perpendicular to the smectic layers. Likewise, $q_\perp$ is the scattering wave vector component perpendicular to the smectic wave vector. $\xi_\parallel$ ($\xi_\perp$) is the correlation length parallel (perpendicular) to the smectic mass density wave vector. It should be noted that because of the anisotropic nature of the fluctuations arising from the splay elastic distortion, a fourth-order term ($\sim q_\perp^4$) is needed to fit the data [28]. The fourth-order term scaling constant c decreases as the temperature ap-

proaches the N-SmA transition temperature and is generally between 0.25 and 0. The thermal term amplitude σ_1 is proportional to the connected susceptibility of the material. The critical behaviors of the heat capacity and the susceptibility show good internal agreement in pure LC systems, especially for those with large nematic ranges [29]. Specifically, the correlation volume exhibits model 3D XY behavior remarkably well [30]. However, because of the QLR nature of the smectic phase, which is described by a power-law singularity, it is not possible in the pure materials to measure the critical behavior of the susceptibility and the order parameter below the transition temperature. In the previous analysis of LC+aerosil x-ray scattering data, the perpendicular correlation length $\xi_\perp$ and the fourth-order term constant c were calculated from $\xi_\parallel$ assuming that the relative power-law dependences observed in the pure LC x-ray scattering data for $T > T_{NA}$ held for the LC+aerosil systems at all temperatures.[1] This assumption only affects the observed longitudinal profile in second order.

In the analysis of our 4O.8+aerosil gel scattering data, we start from Eqs. (1) except that we relax some of the previous assumptions. The most significant change in the new lineshape analysis is that the static longitudinal correlation length is assumed to be distinct from the thermal correlation length. This is, for example, the situation which would be obtained if the transition were into a smectic Bragg glass (SBG) phase. Thus, the static term may be treated entirely independently. It turns out that the peak profile in the smectic-A phase is rather insensitive to the fourth-order term. Therefore, in the analysis presented in this paper, this quadratic term has been omitted in the static part to simplify the structure factor. In the analysis, we have fitted simultaneously all of the scans at various temperatures for a given sample. That is, a complete data set on one ρ_s sample, containing 30–35 different temperature scans, is fitted simultaneously with both temperature-dependent and temperature-independent variables (global variables). Importantly, we have found empirically that the static longitudinal correlation lengths may be fixed at their lowest temperature values.

The cross section then becomes

$$S(\boldsymbol{q}) = S^{thermal}(\boldsymbol{q}) + S^{static}(\boldsymbol{q}), \tag{2a}$$

$$S^{thermal}(\boldsymbol{q}) = \frac{\sigma_1}{1 + (q_\parallel - q_0)^2 \xi_\parallel^2 + q_\perp^2 \xi_\perp^2 + c q_\perp^4 \xi_\perp^4}, \tag{2b}$$

$$S^{static}(\boldsymbol{q}) = \frac{a_2(\tilde{\xi}_{\parallel 2} \tilde{\xi}_{\perp 2}^2)}{[1 + (q_\parallel - q_0)^2 \tilde{\xi}_{\parallel 2}^2 + q_\perp^2 \tilde{\xi}_{\perp 2}^2]^2}. \tag{2c}$$

Again, the measured cross section corresponds to the spherical average of Eqs. (2) since there is no orientational long-range order. In Eq. (2c), the tilde correlation lengths in the static term are fitted to values which are assumed to be constant for all temperatures.

The fit procedure follows the same steps described in previous studies [16–19]. As noted above, because of the orientational isotropy, it is necessary to carry out an average over all angles of Eqs. (2) in order to compare the model cross section with the experimental data. This is, in essence, a microcrystal model for the smectic-A structure factor. This spherically averaged structure factor is then convoluted with the 3D instrumental resolution function. The powder averaging of the model and the convolution are performed numerically. The result is fitted to the experimental data with a temperature-independent background function using a nonlinear least-squares fit routine. As in previous LC+aerosil gel studies, the background is chosen as a constant plus a Porod term which describes the scattering from the Kapton windows, air, and mostly the aerosil particles [16–19]. A Porod background has been confirmed for aerosil gels from small-angle x-ray scattering (SAXS) measurements [15,31]. The functional form is thus $b_P/q^4 + b_C$. The typical q range was chosen to be between ~ 0.1 Å^{-1} and ~ 0.35 Å^{-1} for the analysis, even for scans in the SmA_m phase. The analysis over a wide range of q was necessary in order to distinguish the tails of the smectic peak from the background [9,17].

The Kapton film, which was used as windows of the LC cell, has a broad scattering peak at $q \cong 0.4$ Å^{-1}, outside of the selected range. In order to improve the background determination, the whole data set was also analyzed with a more complex background function which included the Kapton scattering. The latter did not produce any significant differences in the overall results [9].

Each data set was fitted several times with different temperature-dependent and temperature-independent (global) variables. One of the global parameters used in this study is $m_\nu = \nu_\perp / \nu_\parallel$, the ratio of the perpendicular and parallel correlation length critical exponents. The value $m_\nu = 0.81$ for pure 4O.8 was used as a starting value for the fits [28]. When m_ν was allowed to vary with ρ_s, large nonmonotonic variations were observed? The data set was also analyzed assuming $m_\nu = 1$(fixed)—that is, isotropic critical behavior. It turns out that the quality of the fits and the overall χ^2 are insensitive to the explicit assumptions concerning m_ν. For simplicity, in the final fits we fixed $m_\nu = 0.81$, and the ratio of the bare lengths was also fixed at the pure system value. Representative fits are shown in Figs. 2–4. It is evident that Eq. (2) with minimal adjustable parameters $[\sigma_1(T), \xi_\parallel(T), a_2(T), q_0(T), \tilde{\xi}_\parallel]$ plus an assumed temperature-independent background works extremely well. The results obtained from these fits are listed in Table I. As noted above, the perpendicular correlation lengths in both the thermal and static terms of the structure factor are calculated from the longitudinal correlation length assuming the pure 4O.8 critical behavior for the ratio $\xi_\perp / \xi_\parallel$. The results of an analysis in which $\tilde{\xi}_{\perp 2}$ is fitted as a freely adjustable global variable are discussed later in Sec. III E.

We also analyzed the data using Eqs. (1); in general, the results for the parallel correlation lengths at the lowest temperatures, $\xi_\parallel^{LT}$, agree very well with the $\tilde{\xi}_{\parallel 2}$ values deduced using Eqs. (2). However, overall, Eqs. (2) give lower values for χ^2 and also a clearer picture of the behavior around the nematic to smectic-A transition, as we shall discuss below.

Finally, we have carried out a limited number of fits in which the static term, Eq. (2c), is chosen as a Gaussian- rather than Lorentzian-squared function. The overall behav-

[1] T_{NA} is the N-SmA phase transition temperature for the pure LC.

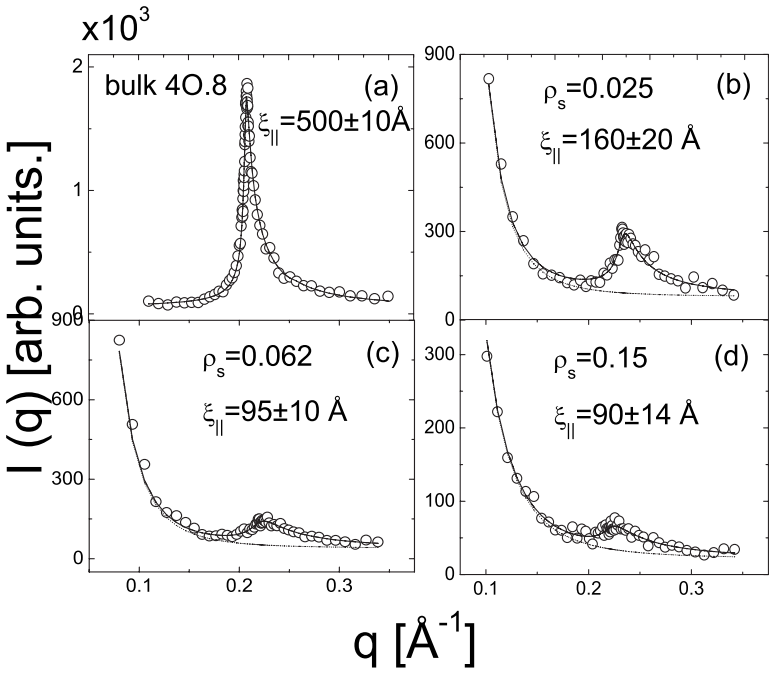

FIG. 4. Scattering intensity $I(q)$ of the pretransitional smectic fluctuations in bulk 4O.8 [panel (a)] and in three different 4O.8+aerosil gels. The intensities for panels (b), (c), and (d) are normalized according to the a_2/b_P ratios given in Table I. The dotted lines show the background. All of the scans are measured at $T=338.15$ K, except the bulk 4O.8 sample which is measured at $T=337.15$ K. The solid lines show the fit results of the thermal structure factor (plus the background) given by Eq. (2a). The best-fit values of the calculated parallel correlation lengths are given in the panels.

ior is closely similar to that obtained with the Lorentzian squared except, of course, the lengths so deduced are larger because of the differences in definition of the underlying intrinsic lengths. Generally, the Lorentzian-squared static cross section yields lower values for the χ^2 although the Gaussian fits are quite good overall. We will discuss the physical significance of the parameters deduced from the varied cross sections in section IV.

B. Pretransitional smectic fluctuations

We show in Fig. 4 the pretransitional smectic fluctuations in the nematic phase for bulk 4O.8 and for samples with three different values of ρ_s. As may be seen from this figure, the presence of the aerosil changes the background dramatically. This can be seen by comparing panels (a) and (b) where for (a) only a linear background is needed. These pretransitional smectic peaks are analyzed by using the thermal structure function given in Eq. (2b) with the static amplitude a_2 set to zero in Eq. (2c). The variables σ_1, q_0 and $\xi_\parallel$ are all temperature-dependent fit parameters. As is evident in Fig. 4, the peak intensity decreases with the increase in aerosil density ρ_s.

C. Smectic x-ray peak position

As may be seen from the high-temperature peak profiles in Figs. 2(a) and 4(b)–4(d), the smectic fluctuations in the nematic phase produce very weak scattering. Because of the poor statistics, fits to the high-temperature data generally involve large uncertainties for the peak positions. This is illustrated for four different aerosil densities in Fig. 5(a) in the

TABLE I. Parameters for nine 4O.8+aerosil gel samples. Shown are the density ρ_s in g/cm^3, the mass of aerosil per volume of LC; the pore volume fraction ϕ; the parallel correlation length of the static term of the structure factor $\tilde{\xi}_{\parallel 2}$ in Å; the order parameter exponent β; low-temperature static amplitude $a_{2\mathrm{LT}}$ (the average of two lowest temperatures) normalized by the Porod amplitude $b_P(\times 10^{-4})$; and the transition temperature T^* in K. $\tilde{\xi}_{\parallel 2}$ is assumed to be independent of temperature.

ρ_s	ϕ	$\tilde{\xi}_{\parallel 2}$	β	$a_{2\mathrm{LT}}/b_P$	T^*
0.025*A*	0.99	15200 (600)	0.23 (2)	3.64 (8)	334.29 (2)
0.025*B*	0.99	16500 (750)	0.25 (2)	2.85 (9)	334.28 (2)
0.040*A*	0.98	9800 (200)	0.25 (2)	2.69 (7)	334.05 (3)
0.040*B*	0.98	8000 (200)	0.25 (2)	2.31 (5)	334.1 (1)
0.062	0.97	3970 (150)	0.22 (1)	1.46 (3)	333.61 (5)
0.096	0.96	3250 (100)	0.26 (2)	0.98 (4)	333.2 (1)
0.15*A*	0.93	1260 (30)	0.31 (3)	0.53 (1)	333.1 (1)
0.15*B*	0.93	1230 (35)	0.31 (2)	0.5 (1)	333.3 (1)
0.3	0.88	580 (15)	0.38 (4)	0.27 (1)	332.9 (1)

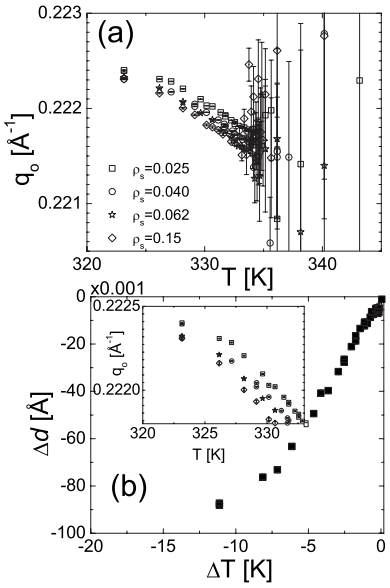

FIG. 5. Temperature dependence of the smectic-A_m peak position and corresponding layer thickness. The layer thickness $d(T)=2\pi/q_o(T)$ is calculated for $\rho_s=0.025$ from its peak positions, and $\Delta d=d(T)-d(T^*)$ is plotted with respect to $\Delta T=T-T^*$, where T^* is the effective critical T_{NA} transition temperature.

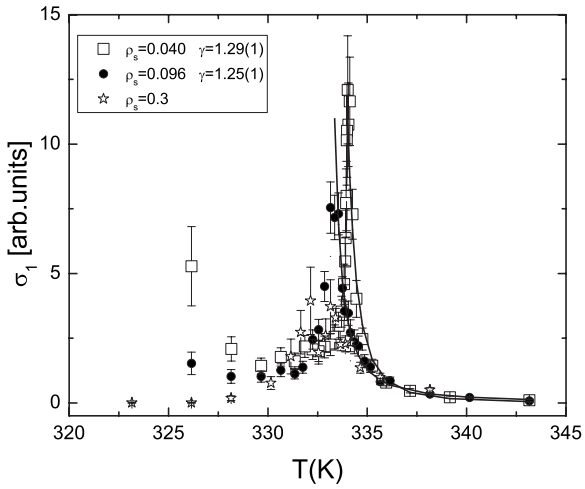

FIG. 6. The thermal amplitude of the structure factor versus temperature for three aerosil densities. Since the thermal amplitudes decrease with an increase in the disorder in the gels, the amplitudes of the $\rho_s=0.096$ and $\rho_s=0.3$ samples are multiplied by 3 and 5, respectively. The solid lines are the results of power-law fits with $\sigma_1 \approx (T^*-T)^{-\gamma}$ to the data above T^* with γ exponents as specified.

temperature range $T>T^*(\rho_s)$. However, once the smectic correlations are well developed, the smectic peaks are concomitantly sharp and q_0 may be determined precisely. Throughout the smectic phase, as seen more clearly from the inset graph of Fig. 5(b), there is a monotonic increase in q_0 on cooling. In this regime, the peak positions are very weakly dependent on aerosil density. Relative to the peak position in pure 4O.8 [28]—that is, $q_0(4O.8)=0.2222(1)$ Å^{-1}—the change in the peak positions for the aerosil gel is less than ~0.1%. This is consistent with the results of a similar study on 8CB+aerosil [16,17]. Thus it can be concluded that the aerosil dispersion does not significantly alter the layer spacing of the smectic A_m in 4O.8 LC. Unexpectedly, the temperature dependence of the layer thickness of 4O.8+aerosil gels is similar to the behavior seen in smectic A_d LC gels like 8CB+aerosil or 8OCB+aerosil. This is shown for the $\rho_s=0.025$ sample in Fig. 5(b). In this figure $\Delta d=d(T)-d_c$ versus $\Delta T=T-T^*(\rho_s)$ is plotted, where d_c is the layer thickness at the N-SmA transition temperature. As discussed in Sec. III E, the transition temperatures T^* (listed in Table I) are calculated using Eq. (3). The variation in Δd with respect to ΔT indicates a positive linear thermal expansion coefficient $\alpha_\parallel$ in contrast to the negative $\alpha_\parallel$ which was observed for the SmA_m LCs $\bar{8}$S5 and $\overline{10}$S5 [32,33]. This difference may be related to the fact that 4O.8 has a rigid link between the rings in its core in contrast to $\bar{n}$S5 LCs which have flexible links.

D. Thermal fluctuations and the thermal correlation length

The structure factor given by Eqs. (1) has only temperature-dependent parameters, except for the background. Most importantly it has a single correlation length to determine both the thermal and static correlations. Fits to Eqs. (1) yield a parallel correlation length which increases continuously with decreasing temperature below the transition and saturates at a value which characterizes the random static correlations in the disordered LC medium. In general, in fits to Eqs. (1) the two amplitudes of Eq. (1b) and (1c) are strongly correlated. This results in large correlated fluctuations of a_2 and σ_1, making it difficult to determine them reliably.

In this study, as discussed in Sec. I, this problem is resolved by decoupling the two parts of the function and using two distinct correlation lengths, given in Eqs. (2b) and (2c). The parallel correlation thermal length $\xi_\parallel$ and the thermal amplitude σ_1 are considered to be temperature-dependent parameters. The static correlation length is treated as temperature independent. The results for the static susceptibility are described in the next section. The fitted values of σ_1 and $\xi_\parallel$ are shown in Fig. 6 and 7 for three different values of ρ_s. The corresponding perpendicular thermal correlation lengths are calculated assuming that the ratio of $\xi_\parallel/\xi_\perp$ is the same as that in pure 4O.8 [28].

As may be seen in Fig. 6 the thermal amplitude σ_1 exhibits pseudocritical behavior both above and below T^*. This behavior is in good agreement with the results of heat capacity measurements [8]. Detailed analysis shows that an increase in the aerosil mass density of the samples suppresses the thermal fluctuations and decreases the thermal amplitude. Because of this decrease, the amplitudes for $\rho_s=0.096$ g/cm^3 and $\rho_s=0.3$ g/cm^3 are multiplied by 3 and 5, respectively, in Fig. 6. It should also be noted that especially for the lowest-density samples it is difficult to determine σ_1 and $\xi_\parallel$ in the smectic-A phase where the scattering is dominated by the static part of the structure factor. Thus only the high-temperature data—i.e., $T>T^*(\rho_s)$—may be fitted to power laws, as indicated by the solid lines in Figs. 6 and 7.

In Fig. 8 the thermal correlation lengths are shown for four different 4O.8+aerosil gel samples as a function of re-

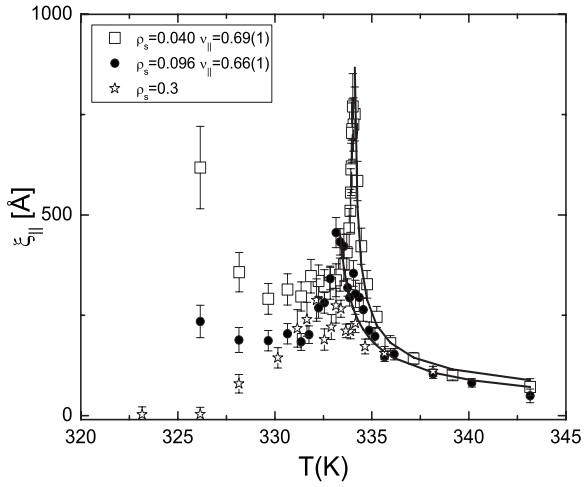

FIG. 7. Thermal correlation lengths versus temperature. The solid lines are the results of power-law fits with $\xi_{\|} \approx (T^* - T)^{-\upsilon_{\|}}$ of the data above the T^* with $\upsilon_{\|}$ exponents as specified.

duced temperature $t=(T-T^*)/T^*$. The pure 4O.8 correlation length is shown as a solid line. As is evident in the figure, there is a systematic deviation of the fitted values of $\xi_{\|}$ from the pure 4O.8 values as t becomes small. There is a plateau indicating saturation starting at $t \cong 5 \times 10^{-4}$ and $t \cong 5 \times 10^{-3}$ for the lowest and highest disordered samples, respectively. The correlation lengths at these plateaus are $\sim 1.5-3$ times smaller than the corresponding l_0 void size of the aerosil network calculated for each ρ_s [34] and about 3–18 times smaller than the limiting smectic correlations length in the Sm*A* phase for the high and low densities, respectively.

E. Static fluctuations and static correlation lengths

As stated above, the two parts of $S(\boldsymbol{q})$ are decoupled by using two different parallel correlation lengths as shown in Eq. (2). As a result, the nonmonotonic variations in the correlation lengths and the amplitudes seen in previous analyses

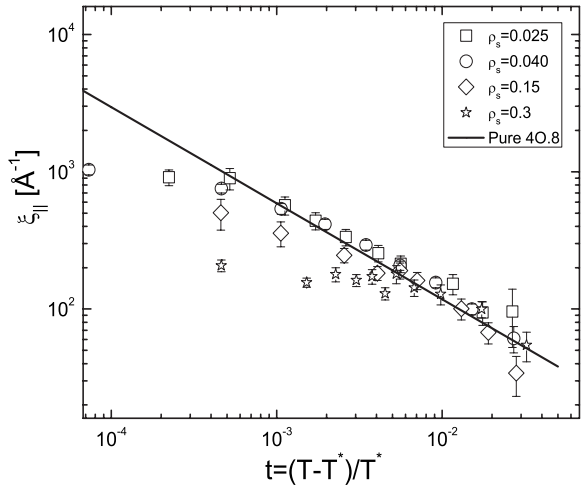

FIG. 8. Thermal correlation lengths of four different aerosil density samples, specified in the figure, versus reduced temperature. The data shown are for the smectic fluctuations above $T^*(\rho_s)$.

due to the coupling between these parameters are decreased noticeably. In the present study, the static term amplitude a_2 is essentially zero in the high-temperature nematic phase. This means that the thermal term of $S(\boldsymbol{q})$, Eq. (2b), describes well the x-ray scattering peaks measured in the nematic phase, as shown in Figs. 2, 9, and 10. To facilitate the fits, a_2 is set to zero for the high-temperature scans above 338 K. Since the *N*-Sm*A* transition for pure 4O.8 is $T_{NA}=336.92$ K and $T^*(\rho_s) < T_{NA}$, setting $a_2=0$ does not alter any results and helps increase the fit stability of the other parameters. The behavior of the structure factor as the temperature is lowered into the Sm*A* phase is shown in Figs 2, 9, and 10. As is evident from these figures, the static contribution grows rapidly below a temperature which is close to, but lower than, T_{NA}. The solid lines are the results of fits to Eq. (2) at each temperature for the different samples. The values of a_2 obtained for four different aerosil densities are shown as functions of temperature in Fig. 11. Figure 12 displays the low-temperature static amplitude $a_{2\mathrm{LT}}$ as a function of ρ_s. Here, $a_{2\mathrm{LT}}$ is the average of the static amplitude for the lowest two temperatures. The low-temperature a_2 values are normalized by the Porod amplitude b_P to account for the volume of the sample in the beam. The solid line in Fig. 12 is the power-law form $a_{2\mathrm{LT}}/b_P \sim \tilde{\rho}_s$ where $\tilde{\rho}_s$ is the reduced aerosil mass density which can be given as $(1-\rho_s)/\rho_s$. This implies that the scattering intensity is proportional to the LC mass in the x-ray beam path [9] as one would expect.

At low temperatures the static term of $S(\boldsymbol{q})$ totally dominates over the thermal term in the fits as shown in Figs. 2, 9, and 10. The dashed lines in these figures correspond to the thermal term contribution plus the Porod background which contributes significantly only to the tails of the smectic peaks. Since a_2 is proportional to the integrated intensity of the static term, $a_2(T)$ can be considered as proportional to the square of the order parameter. The solid lines in Fig. 11 drawn for four different aerosil gels are the results of power-law fits with

$$a_2 \sim (1 - T/T^*)^{2\beta}. \tag{3}$$

This behavior of the order parameter is consistent with the results of previous LC+aerosil x-ray scattering experiments, but the results here are much clearer because of both the density of data points and the improved method of data analysis. The values for β and T^* obtained from the fits are given in Table I and discussed in the next section. The inset of Fig. 11 is drawn to demonstrate the rounding effect of the order parameter for $\rho_s=0.040$ g/cm^3. These data were fitted using a Gaussian distribution of transition temperatures in Eq. (3). The full width at half maximum for $\rho_s=0.040$ g/cm^3 is found to be ~ 0.17 K. As discussed in Ref. [17], the deviation from the expected power-law behavior in highly disordered samples may be due in part to the finite size of domains reached at $t \approx 1 \times 10^{-3}$. The size of the smectic domains will in turn be limited by the nematic correlation length as well as any additional effects of the positional random fields. The rounding will also include any effects of macroscopic heterogeneity in the gel. The transition temperatures, listed in Table I, show a systematic decrease with an

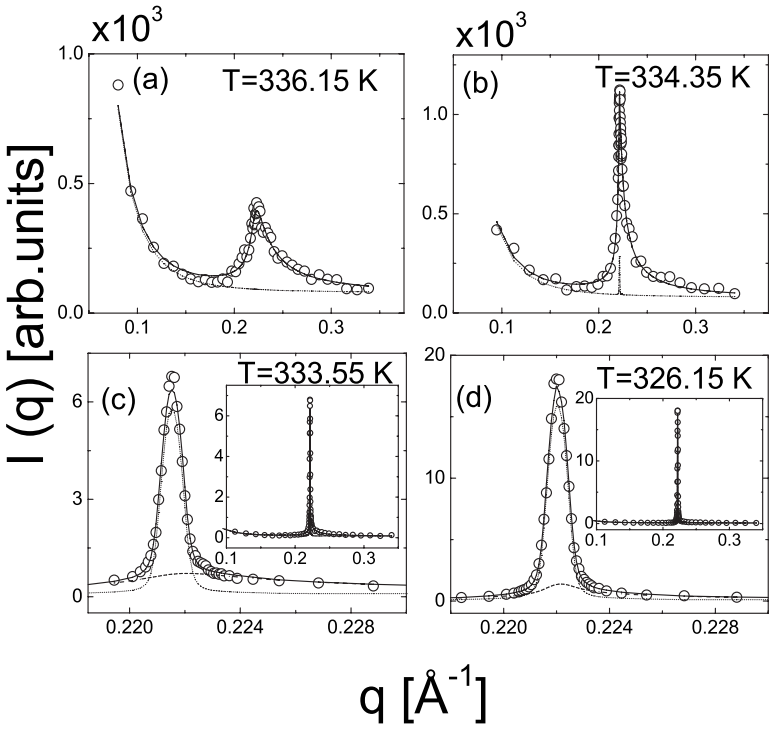

FIG. 9. Scattering intensity $I(q)$ for the least disordered 4O.8+aerosil gel, $\rho_s=0.025$, shown as the sample cools down. The solid lines represent the results of the fits with the model given by Eq. (2), plus the background. As seen in panel (a), the fit is achieved using only the $S^{thermal}$ term. The static part of the structure factor begins to contribute by panel (b) and defines the peak at low temperatures while $S^{thermal}$ describes the tails of the peaks as is evident in panels (c) and (d).

apparent precipitous drop of about 2 K from the pure 4O.8 transition temperature as shown in Fig. 13.

The static parallel correlation lengths $\tilde{\xi}_{\|2}$, obtained as global parameters, are shown in Fig. 14 as a function of aerosil mass density. These values are also given in Tables I and II. The values of $\tilde{\xi}_{\|2}$ extracted from the fits are larger by about a factor of 3 than ℓ_0, the calculated mean void size of the aerosil network [16], as was also observed in 8CB and 8OCB studies [17–19]. Unlike the results of disordered 8CB and 8OCB studies, 4O.8+aerosil analysis reveals a somewhat different scaling exponent for the $\tilde{\xi}_{\|2} \sim \rho_s^{-y}$ relation. The thick solid line in Fig. 14 gives $y=1.4(1)$ for our 4O.8+aerosil gel experiment while the dashed line shows the combined behavior of 8OCB+aerosil and 8CB+aerosil gels with $y \approx 1$. Interestingly, the effective exponent y for the smectic correlation length in the 4O.8+aerosil gel is close to that of the nematic correlation length determined in the 6CB+aerogel system, which has $y_{6CB} \cong 1.6(1)$. In the 6CB+aerogel experiment [35] the nematic correlation length was measured using light scattering. The measured nematic correlation length values are about 7 times larger than 4O.8+aerosil smectic correlation length. The finite size of the nematic correlation length is consistent with the prediction of Radzihovsky and

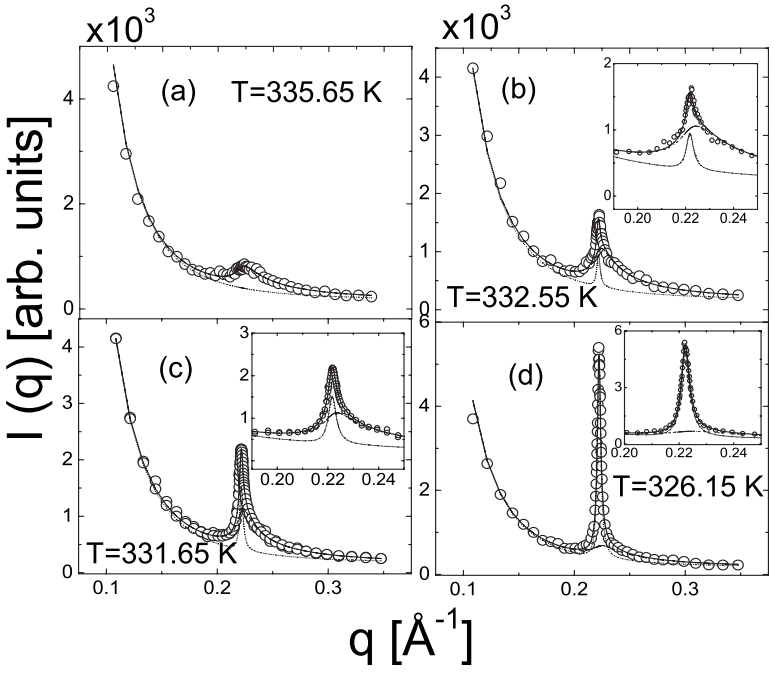

FIG. 10. Scattering intensity $I(q)$ for the most disordered 4O.8+aerosil gel, $\rho_s=0.3$, obtained on cooling. The solid lines show the fits with the total structure factor plus the background. As seen in panel (a), the fit is achieved with only the $S^{thermal}$ term. This part of the structure factor diminishes in panel (d) (low temperatures) where almost all the scattering is modeled by S^{static}. The relative contribution of the two parts of the structure factor can be easily seen in the inset figure of panels (b) and (c).

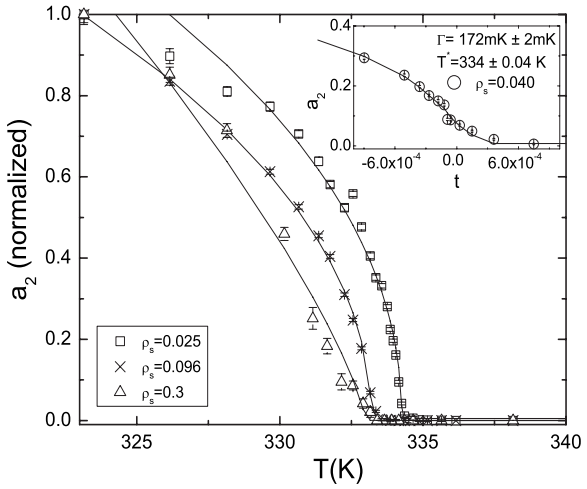

FIG. 11. Normalized static amplitude of the structure factor versus temperature. The solid lines are the power-law fits with Eq. (3), as described in the text. The data are shown for four different density aerosil samples. The inset figure shows the rounding effect seen in the $\rho_s=0.040$ gel (sample *B*). The Gaussian distribution used in the power-law fit for this sample yields a FWHM of ~172 mK for the observed rounding of T^*.

Toner [11] for the effects of the random tilt field.

We also carried out some fits in which the static perpendicular correlation lengths, $\tilde{\xi}_{\perp 2}$ were treated as independent freely adjustable global variable. The results are shown in Table II.

The agreement between $\tilde{\xi}_{\|2}$ values extracted from the two types of fitting analyses is compelling. This shows that $\tilde{\xi}_{\|2}$ is a robust fitting parameter and the line shape is primarily given by $\tilde{\xi}_{\|2}$ while $\tilde{\xi}_{\perp 2}$ has only second-order effects on the line shape. The fit 2 analysis yields noticeably larger values for the putative perpendicular correlation lengths than those used in fit 1. Interestingly, the larger $\tilde{\xi}_{\perp 2}$ values are close to the corresponding values of the mean void size of the aerosil

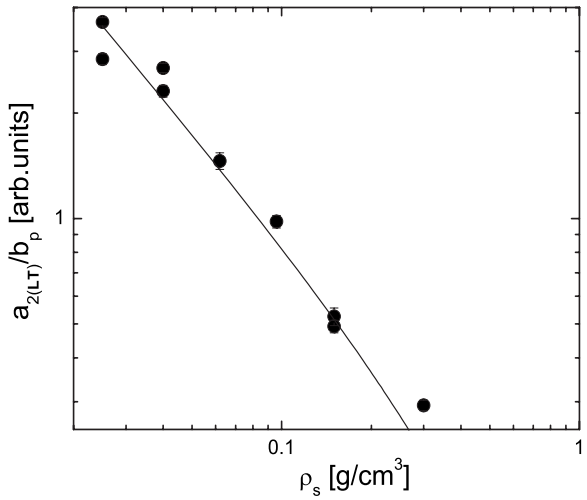

FIG. 12. Normalized static amplitude of the structure factor versus aerosil mass density ρ_s. The line shows the power-law fit with $a_2/b_p \sim \tilde{\rho}_s$ where $\tilde{\rho}_s=(1-\rho_s)/\rho_s$ is the reduced aerosil mass density.

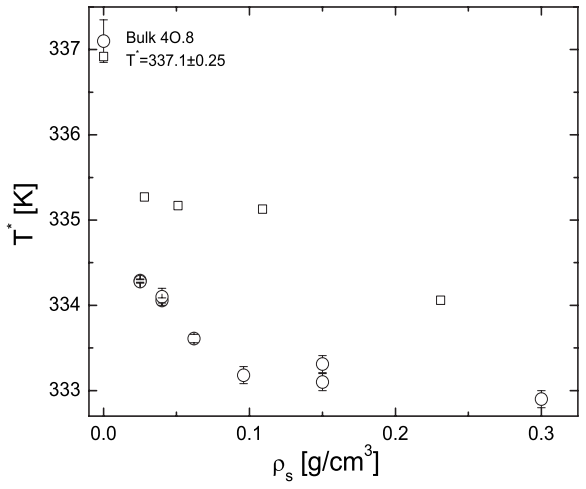

FIG. 13. Transition temperatures versus aerosil mass density. The data represented by the open circles are the results of the present study while the heat capacity results [8] are shown with the open squares.

network $\ell_0 \geqslant \tilde{\xi}_{\perp 2}$. This could be interpreted as a finite-size effect (FSE) where $\ell_0=\xi_M$ is the maximum (cutoff) length scale. This is shown in Fig. 15(b). Here the observed FSE corresponds to the conventional finite-size scaling, argued by Iannacchione *et al.* [16] where the maximum length scale is set by the natural length of the confinement. The mean correlations lengths $\bar{\xi}=(\tilde{\xi}_{\|}\tilde{\xi}_{\perp}^2)^{1/3}$ calculated from the results of the two analyses presented in Table II are shown in Fig. 15(a) as a function of ρ_s. The line shows the mean void size

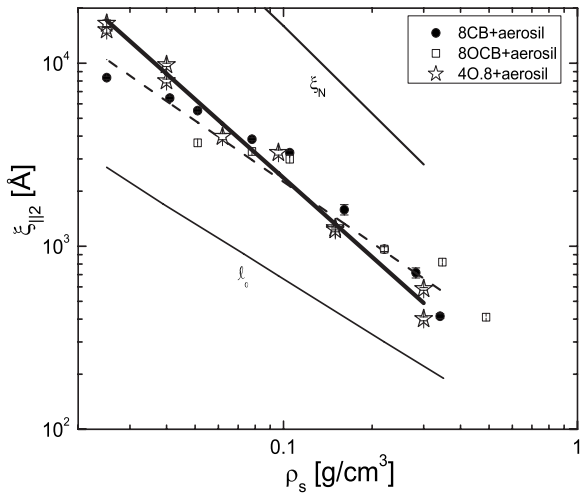

FIG. 14. Static correlation lengths versus aerosil mass density shown for disordered 8CB+aerosil, 8OCB+aerosil, and 4O.8 +aerosil gels. The values shown for 8CB+aerosil and 8OCB +aerosil studies are the average low-temperature correlation lengths which are the results of the analysis using Eq. (1), as described in the text. The static correlation lengths for 4O.8+aerosil gels are the best global fit values $\tilde{\xi}_{\|2}$, which are also listed in Table I. The heavy solid line and the dashed line are the results of power-law fits with $\xi_{\|2} \sim \rho_S^{-y}$. The nematic correlation length for 6CB+aerogel [35] and the calculated void size ℓ_0 for aerosil gels are indicated in the figure.

TABLE II. Static correlation lengths for nine 4O.8+aerosil samples. Shown are the aerosil mass density ρ_s in g/cm^3, the mean void size of the aerosil network ℓ_0, and the static correlation lengths. All length parameters are in Å units. In fit 1, $\tilde{\xi}_{\|2}$ is taken as a global (temperature independent) fit parameter while $\tilde{\xi}_{\perp 2}$ is assumed to have a value set by pure 4O.8 $\xi_\perp(\xi_\|)$ dependence. In fit 2, both $\tilde{\xi}_{\|2}$ and $\tilde{\xi}_{\perp 2}$ are taken to be independently free adjustable global fit parameters.

ρ_s	ℓ_0	$\tilde{\xi}_{\|2}$ Fit 1	$\tilde{\xi}_{\perp 2}$ Fit 1	$\tilde{\xi}_{\|2}$ Fit 2	$\tilde{\xi}_{\perp 2}$ Fit 2
0.025*A*	2700	15200 (600)	902 (65)	14700 (500)	3180 (600)
0.025*B*	2700	16500 (750)	965 (78)	16100 (600)	2200 (300)
0.040*A*	1700	9800 (200)	631 (27)	9700 (150)	1870 (120)
0.040*B*	1700	8000 (200)	535 (15)	8000 (100)	1780 (120)
0.062	1075	3970 (150)	302 (21)	4000 (60)	1100 (130)
0.096	694	3250 (100)	257 (15)	3200 (50)	670 (50)
0.15*A*	444	1260 (30)	119 (5)	1270 (20)	330 (15)
0.15*B*	444	1230 (35)	117 (5)	1300 (20)	410 (20)
0.3	222	580 (15)	63 (3)	580 (10)	140 (8)

of the aerosil network as a function of ρ_s. This can be seen more clearly from the comparison of perpendicular correlation lengths $\tilde{\xi}_{\perp 2}$ (fit 1) and $\tilde{\xi}_{\perp 2}$ (fit 2) in Table II. The ratio of $\tilde{\xi}_\|/\tilde{\xi}_\perp$ for fit 1 is found to be ~17 for the low-ρ_s and ~10 for the high-ρ_s samples. In the second analysis with free global values for $\tilde{\xi}_{\perp 2}$ this ratio is decreased by a considerable amount to ~4 for all aerosil gel samples. Given that the transverse correlation length is not well defined in the LC +aerosil gel systems which is orientationally isotropic, the above analysis is at best suggestive.

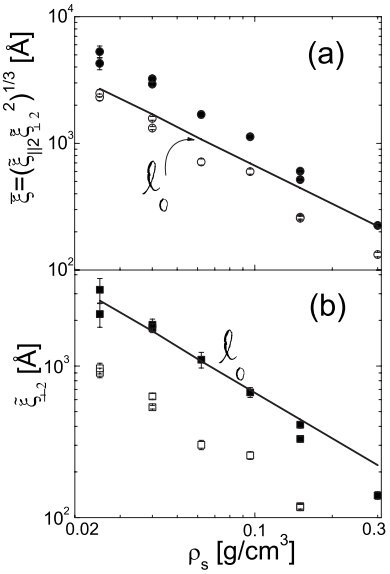

FIG. 15. Volume-averaged static correlation and perpendicular static correlation lengths versus aerosil mass density. Open circles and squares are the values obtained from the fits when $\tilde{\xi}_{\perp 2}$ are calculated from the pure 4O.8 critical behavior. Solid circles and squares are the values from the fits when $\tilde{\xi}_{\perp 2}$ are fitted as free global variables. The solid line is the void size of the aerosil gel, ℓ_0, shown in both panels.

Finally, the results obtained from the fits in which Eq. (2c) is replaced by a Gaussian yield similar results except that the fitted values for $\xi_{\|2}$ are 2–3 times larger than those obtained using the Lorentzian-squared static function. Thus, in the Gaussian model the smectic correlation length in 4O.8 +aerosil gel is approaching the size of the 6CB nematic correlation length in 6CB+aerogel system [35].

IV. DISCUSSION AND CONCLUSION

These 4O.8+aerosil gel experiments have shown that dispersed aerosil, which gelates to form a gel network with 4O.8 in the interstices, significantly affects the phase transition properties of the *N*-Sm*A* transition. Most importantly, the quasi-long-range-order (QLRO) smectic-A_m phase in pure 4O.8 is replaced by a SRO Sm*A* state as a consequence of the quenched random fields imposed by the aerosil gel. This change is observed even for the sample with the weakest disorder, ρ_s=0.025. This is consistent with expectations for the 3D random field *XY* model (3DRF-*XY*) as discussed by many authors [11,36]. In Fig. 14, the static correlation lengths are presented for 8CB+aerosil, 8OCB+aerosil, and 4O.8+aerosil gels. These are the low-temperature (saturated) correlation lengths obtained from the 8CB+aerosil and 8OCB+aerosil studies. The values for the 4O.8+aerosil gel samples have been obtained using the analysis technique discussed above. Essentially all of these analyses yield reliable values for the limiting static longitudinal correlation lengths. These results can be compared with those of Ref. [37] where it was suggested that in the 8CB+aerogel system there may be a second-order phase transition from the nematic phase to a short-range-ordered smectic *A* phase, so-called SBG. Our data seem to be consistent with a second-order transition into a state with a finite positional correlation length except for the rounding of the phase transition close to T^* shown in Fig. 11. However, the rounding is only observed for reduced temperature less than $\sim 2\times 10^{-4}$ and it could arise either from macroscopic inhomogeneities in the sample or from the finite

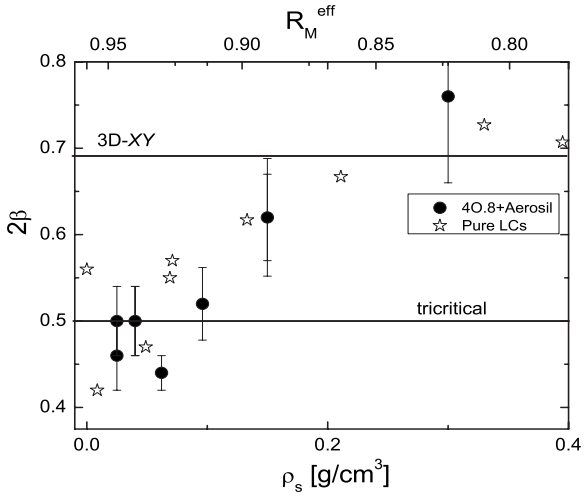

FIG. 16. Critical order parameter exponent obtained from the fits using Eq. (3) versus aerosil mass density. The 2β values for pure LCs were obtained from data given in Ref. [29] and are plotted versus R_M. This allows a comparison of pure LCs and disordered 4O.8+aerosil gels, as discussed in the text.

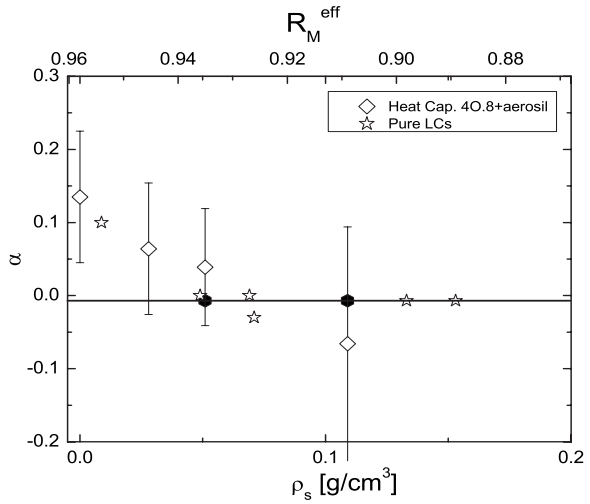

FIG. 17. Heat capacity critical exponent α versus aerosil mass density ρ_s. In order to compare this with the bulk LCs behavior, the same scaling between R_M and ρ_s used in Fig. 16 is also used here. Open and solid diamond data are the measured α values for 4O.8 and three 4O.8+aerosil samples [8]. Stars show α values for the pure LCs, taken from Ref. [29].

nematic correlation length. For a true SBG or *XY* Bragg glass phase, the nematic correlation length must be infinite. Heat capacity data [8] seem to rule out a conventional second-order transition at least for high densities, $\rho_s > 0.1$. The latter may also be affected by macroscopic inhomogeneities. Further work on the possibility of a smectic Bragg glass phase would be invaluable. We should note that recently Liang and Leheny [38] have argued that they observe an *XY* Bragg glass phase in anisotropic 8CB+aerosil gels. They used a modified Gaussian line shape in their analysis. Overall, their results and analyses are consistent with ours. It should also be noted that a similar SBG phase which is predicted to exhibit power-law singularities at the Bragg peak positions has been discussed by Fisher [39].

In Fig. 16, the critical exponents β, extracted from fits to the order parameter using Eq. (3), are shown as a function of ρ_s. The mass density of the aerosil, ρ_s, can be viewed as a parameter which represents the strength of the quenched random field in the sample [16]. However, it should be noted that the exact relation between ρ_s and the disorder field strength Δ caused by the aerosil in LC+aerosil gels is still unknown. Figure 16 gives a comparison of $2\beta(\rho_s)$ for 4O.8 +aerosil with the behavior of effective 2β in pure LCs as a function of the McMillan ratio R_M which is the ratio of the *N*-Sm*A* transition temperature T_{NA} to the *I*-*N* transition temperature T_{IN} ($R_M = T_{NA}/T_{IN}$). This parameter characterizes the strength of the coupling between the nematic order parameter S and the smectic order parameter Ψ (de Gennes coupling). For pure LCs, as the nematic range $\Delta T_N = T_{IN} - T_{NA}$ decreases, R_M approaches 1, the nematic susceptibility increases, and this coupling is strengthened. The result of the strong coupling of the nematic and smectic-*A* order parameters is to drive the *N*-Sm*A* transition toward tricritical and ultimately first-order behavior. As ΔT_N increases, the nematic susceptibility decreases, which makes the coupling weaker and drives the transition towards the 3D *XY* regime. Since smectic phases in pure LCs have QLRO, it is not possible to measure the order parameter directly because of the power-law singularity in the cross section. However, the susceptibility critical exponent γ and the heat capacity critical exponent α are known from x-ray diffraction and from calorimetry measurements, respectively [29]. The corresponding 2β values can be calculated for pure LCs using the Rushbrooke scaling equality $\alpha + \gamma + 2\beta = 2$.

Linear scaling between R_M and ρ_s has been used to compare the behaviors in quenched random disordered 8CB and pure LCs [16,17]. The details of the scaling used in this study are given in Ref. [17] where the concept of an effective McMillan $R_M^{eff}(\text{sil})$ is introduced for a LC+aerosil system. This is defined by $R_M^{eff}(\text{sil}) = R_M^0 - a\rho_s$, where R_M^0 is the McMillan ratio for the pure LC which, in this case, equals 0.958 for 4O.8 LC. The overlay in Fig. 16 was achieved using $a = 0.45$ which is close to the value of $a = 0.47$ used in the 8CB+aerosil study [17]. As may be seen clearly in Fig. 16, an increase in the disorder strength has similar effects on the *N*-Sm*A* critical exponent 2β of 4O.8+aerosil as a decrease in R_M has on that of pure LCs. The nematic susceptibility is suppressed by increased ρ_s, and this in turn drives the *N*-Sm*A* transition towards the 3D *XY* regime. This effect of aerosil dispersion is consistent with the results of previous experiments in which *N*-Sm*A* transitions were studied in 8CB and 8OCB. Figure 17 displays another comparison between the 4O.8+aerosil gel system and pure LCs. In this figure, the heat capacity exponents α obtained from the 4O.8+aerosil calorimetry experiment [8] are shown along with the corresponding α values of pure LCs [29]. With increasing ρ_s, the quenched random field drives the measured critical behavior of the *N*-Sm*A* transition towards the 3D *XY* regime. This result is in agreement with the behavior of $\beta(\rho_s)$.

The static parallel smectic correlation lengths of 8CB, 8OCB, and 4O.8 LC+aerosil gels have been displayed in

Fig. 14 as functions of the disorder strength. These are all based on an assumed Lorentzian-squared cross section for the static susceptibility. As stated in the Results section, the nematic correlation lengths ξ_N for the 6CB+aerogel system are shown by the upper line in this figure. The larger correlation lengths of 6CB are due to the nematic domain size which is physically, by necessity, larger than the size of smectic domains. The values shown for the smectic correlation lengths of 4O.8 are larger than the values of 8CB or 8OCB in the low-density regime. One possible explanation for the larger correlation lengths of 4O.8 at small ρ_s is the molecular structure of the 4O.8 LC. 4O.8 does not have a dipolar group at either end of the molecule unlike 8CB and 8OCB which both have a CN^- terminal group. Thus it is expected that the influence of the aerosil surface anchoring the 4O.8 molecules may be weaker compared to that for 8CB+aerosil and 8OCB+aerosil gels. This could cause the smectic domains of 4O.8 to be less perturbed by the aerosil network, thus allowing larger correlations to grow. This argument was also discussed by Clegg *et al.* [40] for $\bar{8}$S5 which is another nonpolar LC. All of the correlation lengths shown in Fig. 14 are several times larger than the mean void size ℓ_0 of the network. This means that when the smectic domains form, they span many voids in the network.

The scaling of the correlation length as a function of disorder strength Δ has been discussed theoretically by Aharony and Pytte [41]. They deduced the scaling relation $\xi = \Delta^{-1/(d_l-d)}$, where the lower dimensionality of a continuous random field XY system is $d_l=4$. This implies that, for the N-SmA transition which is a typical 3D continuous phase transition ($d=3$), the correlation length dependence on the random variance is $\xi \sim \Delta^{-1}$. Assuming that $\Delta \sim \rho_s$, this yields $\xi_\parallel \sim \rho_s^{-1}$. The corresponding scaling shown in Fig. 14 is $\tilde{\xi}_{\parallel 2} \sim \rho_s^{-1.4(1)}$ for this 4O.8+aerosil study compared with $\xi_\parallel^{LT} \sim \rho_s^{-1.1(1)}$ measured in the 8CB+aerosil study [16]. Given the overall uncertainties in the data we regard this as a satisfactory agreement, especially since the assumption $\Delta \sim \rho_s$ is heuristic.

ACKNOWLEDGMENTS

The authors would like to thank J.L. Jordan-Sweet and K.J. Thomas for assistance during the x-ray scattering measurements. In addition, they would like to thank G.S. Iannacchione and Leo Radzihovsky for helpful discussions. The work at the University of Toronto was supported by the Natural Science and Engineering Research Council of Canada and the work at Lawrence Berkeley Laboratory is supported by the Office of Basic Energy Sciences, U.S. Department of Energy under Contract No. DE-AC03-76SF00098. The National Synchrotron Light Source, Brookhaven National Laboratory is supported by the U.S. Department of Energy under Contract No. DE-AC-02-98CH10886.

[1] T. Bellini, N. A. Clark, C. D. Muzny, L. Wu, C. W. Garland, D. W. Schaefer, and B. J. Olivier, Phys. Rev. Lett. **69**, 788 (1992).
[2] D. E. Feldman and R. A. Pelcovits, Phys. Rev. E **70**, 040702(R) (2004).
[3] L. Wu, B. Zhou, C. W Garland, T. Bellini, and D. W. Schaefer, Phys. Rev. E **51**, 2157 (1995).
[4] N. A. Clark, T. Bellini, R. M. Malzbender, B. N. Thomas, A. G. Rappaport, C. D. Muzny, D. W. Schaefer, and L. Hrubesh, Phys. Rev. Lett. **71**, 3505 (1993).
[5] M. H. W. Chan, K. I. Blum, S. Q. Murphy, G. K. S. Wong, and J. D. Reppy, Phys. Rev. Lett. **61**, 1950 (1988); J. D. Reppy, J. Low Temp. Phys. **87**, 205 (1992).
[6] A. Rappaport, Ph.D. thesis, University of Colorado, 1995.
[7] Z. Kutnjak and C. W. Garland, Phys. Rev. E **55**, 488 (1997).
[8] H. Haga and C. W. Garland, Phys. Rev. E **56**, 3044 (1997).
[9] S. Larochelle, M. Ramazanoglu, and R. J. Birgeneau, Phys. Rev. E **73**, 060702 (2006).
[10] A. Weinberg and B. I. Halperin, Phys. Rev. B **27**, 413 (1983).
[11] L. Radzihovsky and J. Toner, Phys. Rev. B **60**, 206 (1999); Phys. Rev. Lett. **79**, 4214 (1997).
[12] T. Jin and D. Finotello, Phys. Rev. Lett. **86**, 818 (2001).
[13] Z. Kutnjak, S. Kralj, and S. Zumer, Phys. Rev. E **66**, 041702 (2002); A. Hourri, T. K. Bose, and J. Thoen, *ibid.* **63**, 051702 (2001).
[14] M. Caggioni, A. Roshi, S. Barjami, F. Mantegazza, G. S. Iannacchione, and T. Bellini, Phys. Rev. Lett. **93**, 127801 (2004).
[15] G. S. Iannacchione, G. P. Crawford, S. Zumer, J. W. Doane, and D. Finotello, Phys. Rev. Lett. **71**, 2595 (1993).
[16] G. S. Iannacchione, S. Park, C. W. Garland, R. J. Birgeneau, and R. L. Leheny, Phys. Rev. E **67**, 011709 (2003).
[17] R. L. Leheny, S. Park, R. J. Birgeneau, J.-L. Gallani, C. W. Garland, and G. S. Iannacchione, Phys. Rev. E **67**, 011708 (2003).
[18] P. S. Clegg, C. Stock, R. J. Birgeneau, C. W. Garland, A. Roshi, and G. S. Iannacchione, Phys. Rev. E **67**, 021703 (2003).
[19] S. Park, R. L. Leheny, R. J. Birgeneau, J.-L. Gallani, C. W. Garland, and G. S. Iannacchione, Phys. Rev. E **65**, 050703(R) (2002); S. Park, Ph.D. thesis, MIT, 2002.
[20] D. Liang, M. A. Borthwick, and R. L. Leheny, J. Phys.: Condens. Matter **16**, S1989 (2004).
[21] R. E. Peierls, Helv. Phys. Acta **7**, 81 (1934), L. D. Landau and E. M. Liftshitz, *Statistical Physics*, 2nd ed. (Pergamon Press, New York, 1980).
[22] G. S. Iannacchione, C. W. Garland, J. T. Mang, and T. P. Rieker, Phys. Rev. E **58**, 5966 (1998).
[23] Frinton Lab., Vineland, NJ, 08360.
[24] Degussa Corp., Ridgefield Park, NJ, 07660.
[25] Instead of ethanol, pure toluene which has a much higher boiling temperature ~111 °C was also tried as a solvent. The aim was to hold the 4O.8 in its isotropic phase as long as possible while drying to obtain a homogenous dispersion of aerosil. However, the effect of toluene was found destructive on the

aerosil network although it dissolves the aerosil in 4O.8 better than ethanol.
[26] R. J. Birgeneau, J. Magn. Magn. Mater. **177-181**, 1 (1998).
[27] H. Yoshizawa, R. A. Cowley, G. Shirane, R. J. Birgeneau, H. J. Guggenheim, and H. Ikeda, Phys. Rev. Lett. **48**, 438 (1982).
[28] R. J. Birgeneau, C. W. Garland, G. B. Kasting, and B. M. Ocko, Phys. Rev. A **24**, 2624 (1981).
[29] C. W. Garland and G. Nounesis, Phys. Rev. E **49**, 2964 (1994).
[30] C. W. Garland, G. Nounesis, M. J. Young, and R. J. Birgeneau, Phys. Rev. E **47**, 1918 (1993).
[31] D. W. Schaefer and K. D. Keefer, Phys. Rev. Lett. **56**, 2199 (1986).
[32] E. Anesta, G. S. Iannacchione, and C. W. Garland, Phys. Rev. E **70**, 041703 (2004).
[33] G. Cordoyiannis, S. Kralj, G. Nounesis, S. Zumer, and Z. Kutnjak, Phys. Rev. E **73**, 031707 (2006).
[34] The void size is given by $l_0=2/a\rho_s$, where a is the specific surface area for the aerosil (given as $a=300\ \mathrm{m}^2\ \mathrm{g}^{-1}$ for type-300 aerosils). A more detailed derivation can be found in G. Porod, in *Small Angle X-ray Scattering*, edited by O. Glatter and O.Kratky (Academic Press, London, 1982).
[35] T. Bellini, N. A. Clark, V. Degiorgio, F. Mantegazza, and G. Natale, Phys. Rev. E **57**, 2996 (1998).
[36] Y. Imry and S.-K Ma, Phys. Rev. Lett. **35**, 1399 (1975).
[37] T. Bellini, L. Radzihovsky, J. Toner, and N. A. Toner, Science **294**, 1074 (2001).
[38] D. Liang and R. Leheny, e-print arXiv:cond-mat/0611637.
[39] D. S. Fisher, Phys. Rev. Lett. **78**, 1964 (1997).
[40] P. C. Clegg, R. J. Birgeneau, S. Park, C. W. Garland, G. S. Iannacchione, R. L. Leheny, and M. E. Neubert, Phys. Rev. E **68**, 031706 (2003).
[41] A. Aharony and E. Pytte, Phys. Rev. B **27**, 5872 (1983).